Ion charge number and flux saturation effects in the corona of a laser-irradiated pellet

J. Sanz and J.R. Sanmartín
E. T. S. Ingenieros Aeronáuticos, Universidad Politécnica de Madrid, Madrid-3, Spain

(Received 29 December 1981; accepted 29 July 1983)

The quasisteady structure of the corona of a laser-irradiated pellet is completely determined for arbitrary Z_i (ion charge number) and r_c/r_a (ratio of critical and ablation radii), and for heat-flux saturation factor f above approximately 0.04. The ion-to-electron temperature ratio at r_c grows sensibly with Z_i; all other quantities depend weakly and nonmonotonically on Z_i. For r_c/r_a close to unity, and all Z_i of interest ($Z_i < 47$), the flow is subsonic at r_c. For a given laser power W, flux saturation may decrease (low f) or increase (high f) the ablation pressure P_a relative to the value obtained when saturation is not considered; in some cases a decrease in f with W fixed increases P_a. For intermediate f (~ 0.1), $P_a \propto (W/r_a^2)^{2/3} \rho_c^{1/3}$ (ρ_c = critical density), independently of r_c/r_a; for $f \sim 0.6$, P_a is larger by a factor of about $(r_c/r_a)^{2/3}$. For $r_c/r_a > 1.2$ roughly, the mass ablation rate is $C(Z_i)[(m_i/kZ_i)^{7/2}\bar{K}r_a^{11}P_a^5]^{1/6}$, independent of ρ_c and f, and barely dependent on Z_i (m_i is ion mass; k, Boltzmann's constant; $\bar{K}$, conductivity coefficient; and C, a tabulated function).

I. INTRODUCTION

The complex set of phenomena involved in laser fusion is usually studied through thorough numerical simulations. It is clear, however, that simple scaling laws for partial aspects of the entire process would be quite interesting. In the recent past there have been attempts to derive such laws for the corona of plasma ablated from the target, setting aside the problem of target compression. Reasonable approximations introduced in the analysis have been (a) fluid description, (b) spherically symmetric flow, (c) quasisteady flow, (d) classical (Spitzer's) conductivity, and (e) anomalous absorption at the critical density n_c (negligible inverse bremsstrahlung). In the analyses relations were sought between laser power W, wavelength λ (or n_c), instantaneous pellet radius r_a, average ion mass m_i and charge number Z_i, pressure at the cold ablation surface P_a, ablation rate constant μ, radius of critical surface r_c, temperatures T_{ec} and T_{ic}, etc.

The problem was first discussed by Caruso[1] who suggested that, for $r_c/r_a \to \infty$, the critical density n_c, then lying at infinity, would be an ignorable parameter. Later Gitomer *et al.*[2] and Afanas'ev *et al.*[3] carried out detailed analytical studies. Max *et al.*[4] introduced into the problem the usual flux-limit factor f to take into account that flux saturation must occur over part of the corona under a broad range of conditions; they presented a thorough discussion of physical phenomena not included in the analysis. Saturation in a related astrophysical context had been discussed by Cowee and McKee.[5] Nuckolls[6] had earlier suggested how flux saturation would affect the relation $P_a(W)$.

The analysis of Refs. 2 and 3 was reexamined by the authors elsewhere.[7] If r_a, n_c, m_i, and Z_i are given, their dimensionless formulation leads to a two-eigenvalue problem, in which r_c/r_a is a free parameter in the range $(1, \infty)$. One then obtains complete results for W, P_a, μ, etc., in dimensionless form. In particular, elimination of r_c/r_a yields W and μ in terms of r_a, P_a, n_c, m_i, and Z_i; briefly $W(r_a, P_a)$ and $\mu(r_a, P_a)$. The interest of this is that the "inner" problem (the region $r < r_a$, as opposed to the outer one, $r > r_a$) *can* in principle be solved, if $\mu(r_a, P_a)$ is known, for any kind of compression desired, without further consideration of the corona; in each case one would then obtain laws $r_a(t)$, $P_a(t)$, and thus finally $\mu(t)$ and $W(t)$.

The formulation of Ref. 7 showed that the behavior of the far away plasma evolves as W increases (T_e first decaying with distance as $r^{-4/3}$, then as $r^{-2/5}$, and finally as $r^{-2/7}$), with a dramatic effect on the relation $P_a(W)$: When r_c/r_a (or W) is large, the absorbed laser energy is mostly conducted outward, leading to an ablation pressure well below that predicted by Caruso[1]; for r_c/r_a large, n_c is *not* an ignorable parameter. This effect went unnoticed in Ref. 2, where no explicit results were given, and in Ref. 3, where wrong laws were presented ($P_a \propto W^{1/2}/r_a^{7/4}$, $T_{ec} \propto P_a^{2/3} r_a^{3/4}$, etc., for r_c/r_a not too close to unity). Again the special behavior of the solution for r_c/r_a close to unity was either unnoticed[2] or incorrectly determined[3] because the structure of a laser-produced deflagration layer was not taken into account. Finally, Ref. 7 showed that one should let $T_e \neq T_i$ for consistency (times for ion-electron energy relaxation and electron heat conduction being comparable); T_i was decoupled from the problem by assuming Z_i large, and correctly determined at the end. Gitomer *et al.*[2] had set $T_e = T_i$; Afanas'ev *et al.*[3] assumed Z_i large but their T_i was wrong because they did not take into account ion cooling due to expansion.

In the present work we extend the analysis of Ref. 7 to include finite (arbitrary) Z_i values (Sec. II) and flux saturation (Sec. III). In the final discussion of results (Sec. IV) we include a comparison with the analysis and results of Refs. 4 and 6.

 0031-9171/83/113361-10$01.90

II. ARBITRARY ION CHARGE NUMBER

Following the earlier work of Sanz *et al.*,[7] we consider the equations for quasineutral, steady, spherically symmetric flow: mass conservation

$$nvr^2 = \mu, \tag{1}$$

ion–electron momentum conservation

$$m_i n v \frac{dv}{dr} = -\frac{d}{dr} nk(Z_i T_e + T_i), \tag{2}$$

ion entropy

$$\frac{n}{Z_i} T_i v \frac{d}{dr}\left(k \ln \frac{T_i^{3/2}}{n}\right) = \frac{3}{2} kn^2 \frac{T_e - T_i}{\bar{t}_{ei} T_e^{3/2}}, \tag{3}$$

and an overall energy equation which, making use of the boundary conditions at $r_a (v = T_e = T_i = T_e^{5/2}\, dT/dr = 0)$, reads

$$\mu\left(\frac{5}{2} k(Z_i T_e + T_i) + \frac{1}{2} m_i v^2\right) = Z_i r^2 \bar{K} T_e^{5/2} \frac{dT_e}{dr} + \frac{W Z_i H(r)}{4\pi}, \tag{4}$$

$$H = 0 \quad (r < r_c), \quad H = 1 \quad (r > r_c),$$

and is used instead of the entropy equation for electrons. All symbols have the usual meaning.

Defining

$$\eta = \frac{r}{r_a}, \quad \theta_e = \frac{T_e}{T_r}, \quad \theta_i = \frac{T_i}{T_r},$$

$$u = \frac{v}{(Z_i k T_r / m_i)^{1/2}},$$

and choosing T_r in such a way that the boundary condition $P(r_a) = P_a$, using (1), reads

$$u/\theta_e = 1 \quad \text{at } \eta = 1, \tag{5}$$

we find

$$T_r = \left(\frac{Z_i}{1 + Z_i}\right)^2 \frac{Z_i}{m_i k} \frac{P_a^2 r_a^4}{\mu^2}$$

and

$$\frac{1}{2}\left(1 - \frac{\theta_e + 5\theta_i/3Z_i}{u^2}\right)\frac{du^2}{d\eta} = \frac{2}{\eta}\left(\theta_e + \frac{5\theta_i}{3Z_i}\right) - \frac{d\theta_e}{d\eta} - \frac{6.45\, b}{\beta Z_i} \frac{\theta_e - \theta_i}{\eta^2 u^2 \theta_e^{3/2}}, \tag{6}$$

$$\frac{5}{2}\left(\theta_e + \frac{\theta_i}{Z_i}\right) + \frac{1}{2} u^2 = \beta \eta^2 \theta_e^{5/2} \frac{d\theta_e}{d\eta} + \bar{W} H(\eta), \tag{7}$$

$$\beta\eta^2\left(\frac{3}{2} u^2 \frac{d\theta_i}{d\eta} + \frac{2u^2\theta_i}{\eta} + \frac{1}{2}\theta_i \frac{du^2}{d\eta}\right) = 9.68\, b \frac{\theta_e - \theta_i}{\theta_e^{3/2}}, \tag{8}$$

$$H = 0 \quad (\eta < \eta_c), \qquad H = 1 \quad (\eta > \eta_c).$$

Here

$$\beta = \left(\frac{Z_i}{1 + Z_i}\right)^5 \left(\frac{Z_i}{m_i}\right)^{5/2} \frac{\bar{K}}{k^{7/2}} \frac{r_a^{11} P_a^5}{\mu^6}, \tag{9}$$

$$\bar{W} = \left(\frac{Z_i + 1}{Z_i}\right)^2 \frac{m_i}{4\pi Z_i} \frac{\mu W}{P_a^2 r_a^4}, \tag{10}$$

$$\eta_c^2 u(\eta_c) = \frac{Z_i + 1}{Z_i} \frac{m_i}{Z_i n_c} \frac{\mu^2}{P_a r_a^4}; \tag{11}$$

$b(Z_i) \equiv Z_i \bar{K}(Z_i)/\bar{K}(1)$ varies between 1 at $Z_i = 1$ and 4.2 for $Z_i \to \infty$.

The boundary conditions are (5) and

$$\theta_e = 0, \quad \theta_i/\theta_e = 1 \text{ at } \eta = 1,$$

$$\theta_e \to 0, \quad \text{as } \eta \to \infty,$$

together with either one of two conditions,

$$\frac{d\theta_e}{d\eta} = 2\frac{\theta_e + 5\theta_i/3Z_i}{\eta} - \frac{6.45\, b}{\beta Z_i} \frac{\theta_e - \theta_i}{\eta^2 u^2 \theta_e^{3/2}} \tag{12a}$$

or

$$\eta_c = \eta_s, \tag{12b}$$

at the point η_s where $u^2 = \theta_e + 5\theta_i/3Z_i$. Notice that conditions (12), required to avoid multivalued solutions in Eq. (6), occur at a sonic point, partly isothermal, partly isentropic.

As in Ref. 1 we solve Eqs. (6)–(8) choosing as free parameter η_c, in the range $1 < \eta_c < \infty$; for each value we find β, $\bar{W}$, and $u(\eta_c)$, and then through (9)–(11) we arrive at P_a, W, and μ. Now, however, T_i is coupled to both v and T_e.

For $\eta < \eta_c (H = 0)$, we may introduce phase-space variables $Y \equiv \beta\eta\theta_e^{5/2}$, $M^2 \equiv u^2/\theta_e$, together with $\psi \equiv \theta_i/\theta_e$; they obey equations

$$\frac{dY}{d\ln\eta} = F_1(M, \psi, Y), \tag{13}$$

$$\frac{dM^2}{dY} = F_2(M, \psi, Y), \quad \frac{d\psi}{dY} = F_3(M, \psi, Y). \tag{14}$$

Assume first that the flow, which starts as subsonic ($u^2/\theta \sim u \sim 0$ at $\eta = 1$), is supersonic at $\eta_c (\eta_s < \eta_c)$. Condition (12a) shows that the solution must cross the sonic plane π_s,

$$M^2 = 1 + 5\psi/3Z_i$$

at its intersection L_0 with the surface

$$2M^2(Y - 1) - 1 = (6.45\, b/Z_i)\frac{(1 - \psi)}{M^2};$$

L_0 is a line of saddle points. The solution to (14) near its singular point $Y = 0$, $M^2 = 0$, $\psi = 1$, which is part node, part saddle and corresponds to $\eta = 1$, takes the form

$$M^2 \simeq \left(\frac{Y}{\beta}\right)^{2/5}, \quad \psi - 1 = \frac{25(Z_i + 1)}{6 \times 6.45 b Z_i}\left(\frac{Y}{\beta}\right)^{2/5};$$

this one-parameter family of curves intersects π_s in a curve L_s. Sweeping through positive values of β we determine L_s, and thus the value β_l for which it meets L_0 at a point $Y_{sl}, M_{sl}, \psi_{sl}$. The topology of the solutions is shown in Fig. 1: L_s ends at L_0; for $\beta > \beta_l$ the solutions do not reach π_s and the flow stays everywhere subsonic.

Integrating from the point $Y_{sl}, M_{sl}, \psi_{sl}$ into the supersonic half-space, we entirely determine $M^2(Y)$, $\psi(Y)$. Then

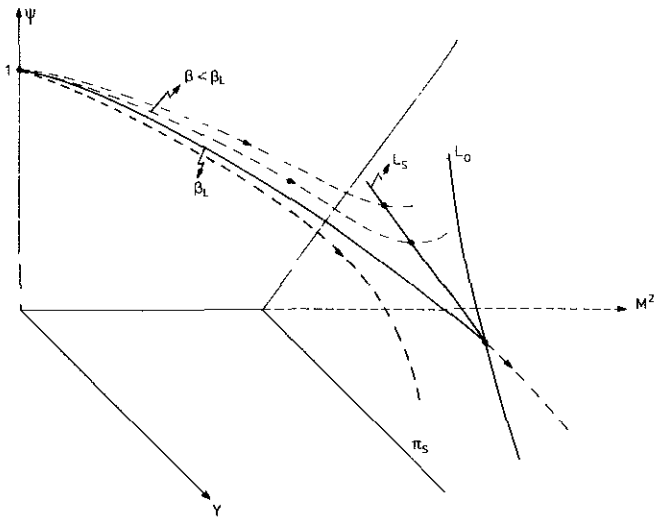

FIG. 1. Topology of integral curves in the phase space of Eqs. (14).

Eq. (13), with the boundary condition $Y = 0$ at $\eta = 1$, yields the sonic radius η_{sl} and $Y(\eta)$, and hence $u(\eta)$, $\theta_e(\eta)$, and $\theta_i(\eta)$ (shown in Fig. 2 for $Z_i = 1$) up to the critical radius η_c, wherever it may be. For any chosen $\eta_c > \eta_{sl}$, all three values $u(\eta_c)$, $\theta_e(\eta_c)$, and $\theta_i(\eta_c)$ are known. Equations (6)–(8) could be integrated, starting at η_c, if $\overline{W}$ were known. The quantity $\overline{W}$ is then determined by the condition at infinity ($\theta_e \to 0$).

As $\overline{W}$ (and η_c) decreases a value $\overline{W}_l$ is reached for which $\eta_c = \eta_{sl}$; both Eqs. (12a) and (12b) are then satisfied. There are two slopes at η_c: Equation (12a) holds clearly at η_c^- ($\eta_s = \eta_c^-$). For $\overline{W} < \overline{W}_l$ (or $\eta_c < \eta_{sl}$) Eq. (12b) must be used instead of (12), that is, the solution corresponds to some value $\beta < \beta_l$. For any such β, integration of (13) and (14) yields η_s, $u(\eta_s)$, $\theta_e(\eta_s)$, and $\theta_i(\eta_s)$. Since $\eta_c = \eta_s$, to solve for the range $\eta > \eta_s$ one proceeds as previously.

As η_c decreases further a value η_{cs} may be found such that Eq. (12a), in addition to (12b), is again satisfied; now (12a) holds at η_c^+ ($\eta_s = \eta_c^+$). For $1 < \eta_c < \eta_{cs}$, Eq. (12a) and not (12b) must be used ($\eta_s > \eta_c$). At η_s (and in general for any $\eta > \eta_c$) one should have $d\theta/d\eta < 0$. This is impossible for $Z_i \to \infty$, when the last term in (12a) vanishes[7]; thus, no such η_{cs} exists for Z_i above some value, which we find numerically to be approximately 46.

As $\eta_c \to 1$, we find $\beta \to 0$; heat conduction is then limited to a thin deflagration layer (adjoining the pellet) which involves large gradients and may be treated as planar.[7] Outside, the flow is isentropic and $T_i = T_e$.

Figures 3 and 4 show P_a vs W, and μ vs P_a, respectively; Fig. 5 gives r_c/r_a, $P(r_c)/P_a$, and $T_i(r_c)/T_e(r_c)$ vs P_a. Figures 6 and 7 relate W to P_a and mass ablation rate ($\dot{m} \equiv 4\pi m_i \mu / Z_i$), and to $T_e(r_c)$ and $T_i(r_c)$, respectively, for particular conditions. Figure 8 and Table I give $r_s(r_c)$, and β_l and η_c^*,[8] respectively, for several values of Z_i.

III. HEAT FLUX SATURATION EFFECTS

When the electron mean free path is larger than the characteristic length for temperature changes, the classical result, $q = -\overline{K} T_e^{5/2} dT_e/dr$, yields unphysically large values of the heat flux. A simple way to correct for this has been to saturate, or limit the value of, q, in the form

$$|q| \leqslant f n k T_e (k T_e / m_e)^{1/2}.$$

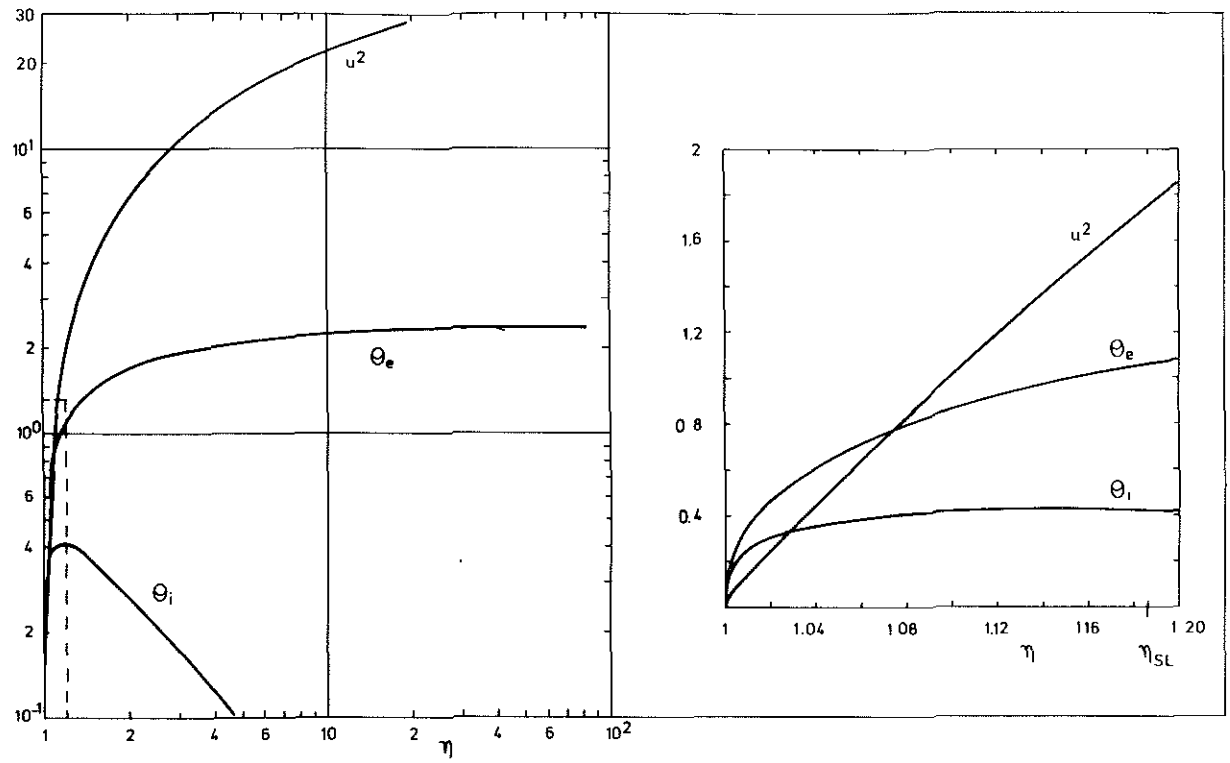

FIG. 2. Dimensionless squared velocity and temperatures versus radius ($\eta \equiv r/r_a$) for $1 < \eta < \eta_c$ and $\eta_{sl} < \eta_c$, and $Z_i = 1$.

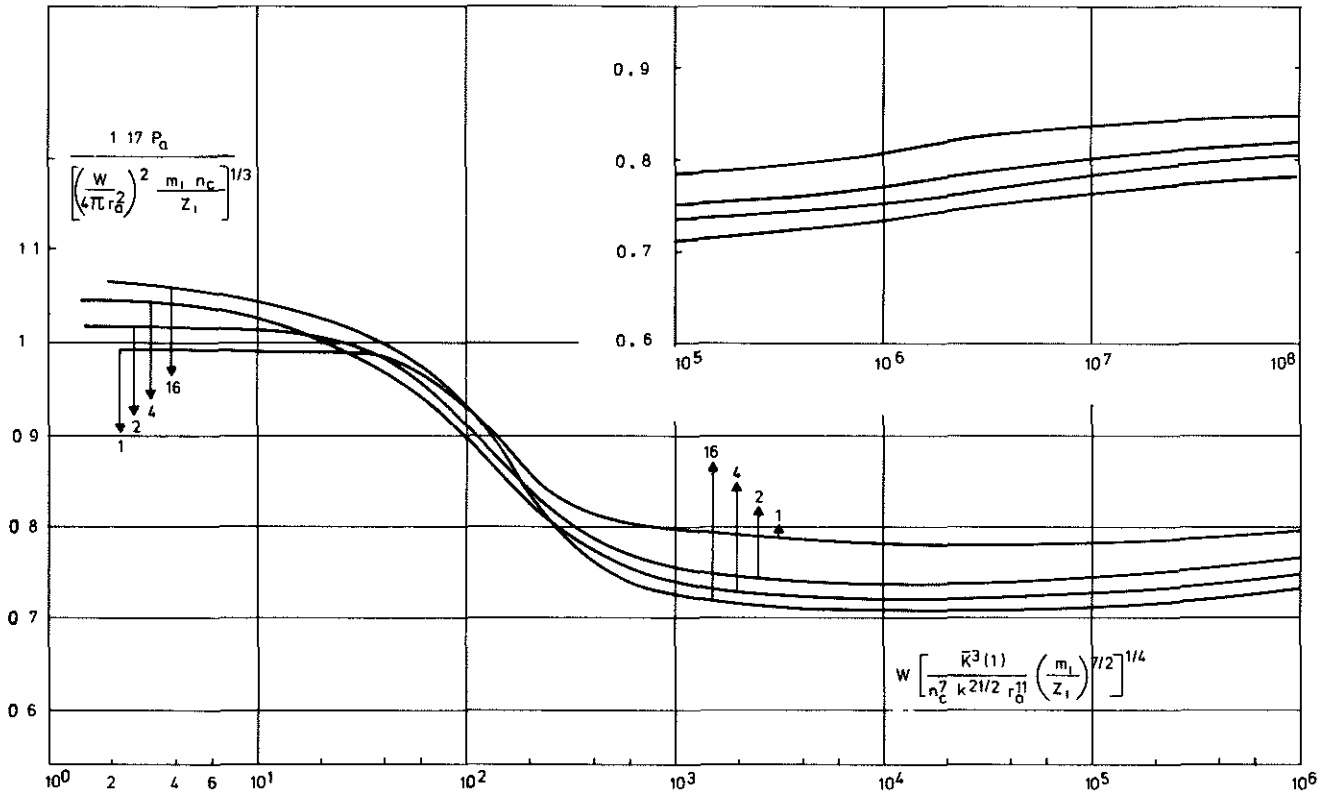

FIG. 3. Ablation pressure P_a versus absorbed laser power W, for $Z_i = 1$, 2, 4, and 16. In convenient units, the horizontal axis is $39.7\, W\lambda^{7/2}(A_i/Z_i)^{7/8} r_a^{11/4}$ and the vertical axis is $0.522\, P_a r_a^{4/3}\lambda^{2/3} W^{-2/3}(Z_i/A_i)^{1/3}$; P_a is measured in 10^6 bars, W in 10^{12} W, λ in μm, and r_a in mm. Here A_i is the ion mass number.

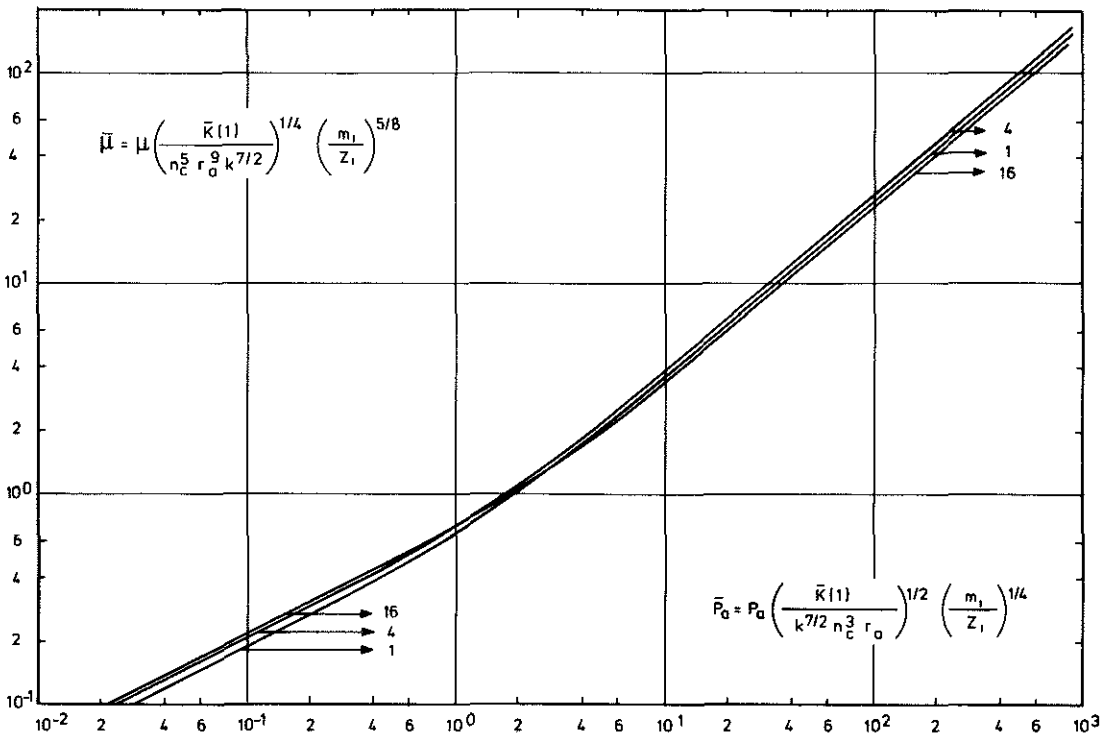

FIG. 4. Mass ablation rate $\dot{m}$ vs P_a for $Z_i = 1$, 4, and 16. The horizontal axis is $0.961\, P_a\lambda^3(A_i/Z_i)^{1/4} r_a^{1/2}$ and the vertical axis is $1.93\times10^{-4}\times\dot{m}\lambda^{5/2} r_a^{-9/4}(Z_i/A_i)^{3/8}$; $\dot{m}$ is measured in g/sec, other units as in Fig. 3.

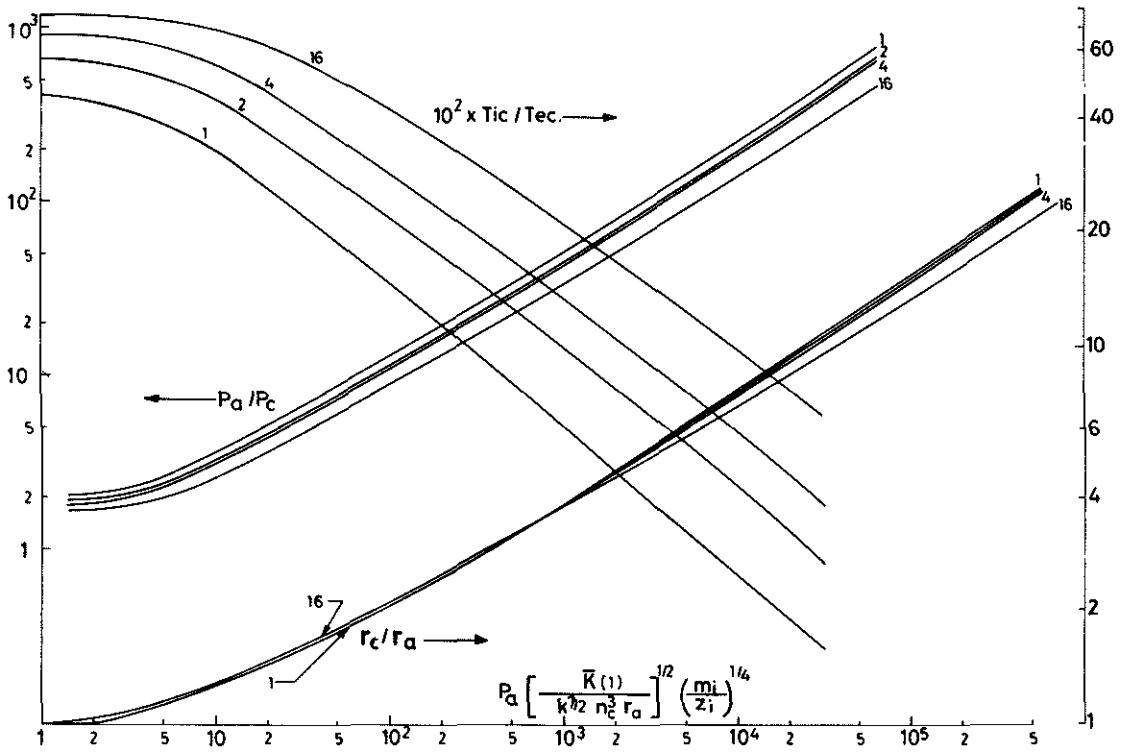

FIG. 5. Ion-to-electron temperature ratio at the critical radius, ablation to critical pressure ratio, and critical to ablation radius ratio, for $Z_i = 1$, 2, 4, and 16; same horizontal axis as in Fig. 4.

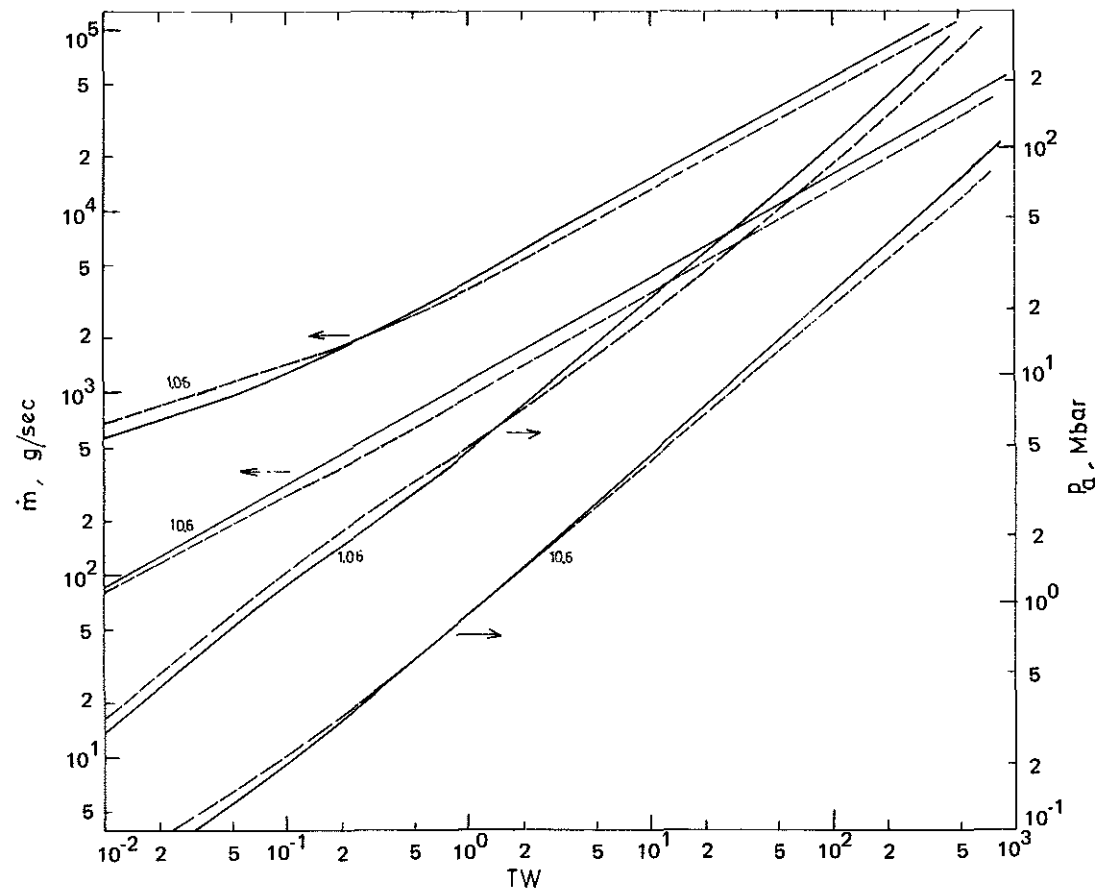

FIG. 6. Mass ablation rate and ablation pressure versus laser power for $r_a = 500$ μm, laser wavelengths $\lambda = 1.06\,\mu$m and $10.6\,\mu$m, $Z_i = 1$ (—) and 16 (– – –), and $A_i/Z_i = 2$. ($TW = 10^{12}$ W).

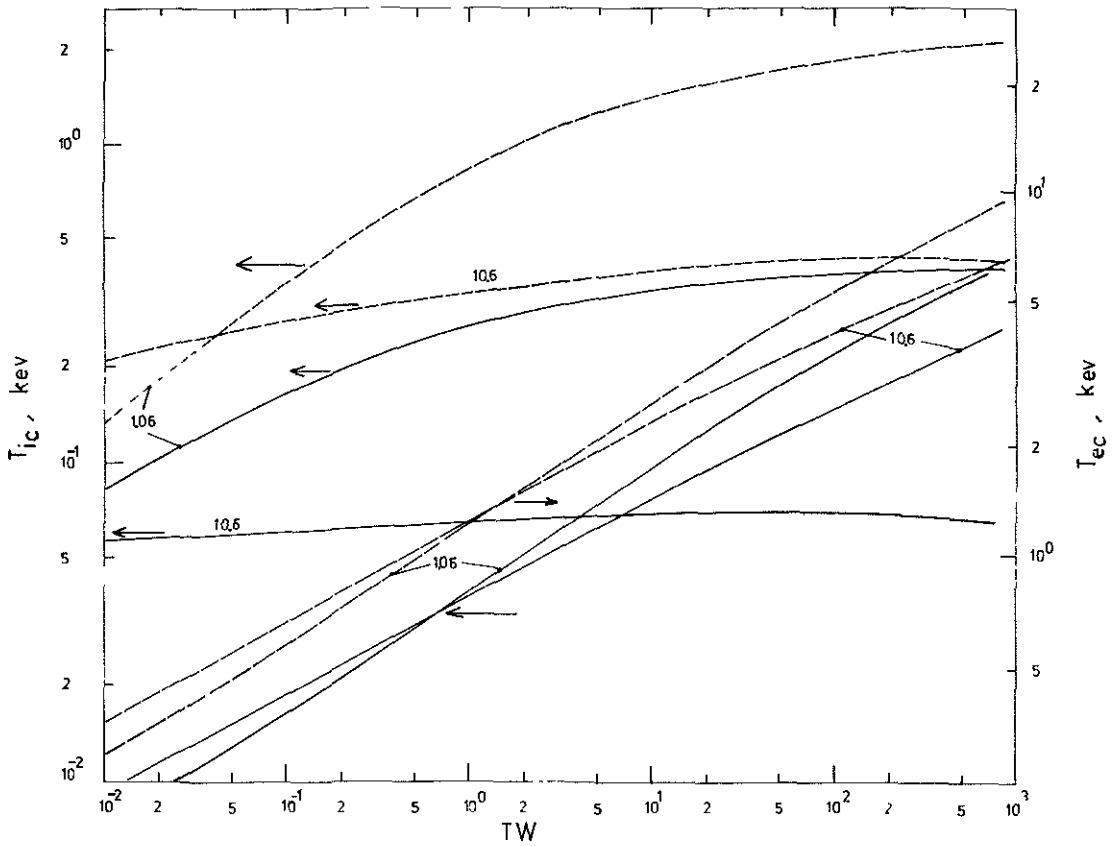

FIG. 7. Ion and electron temperatures at critical radius for the same conditions as in Fig. 6.

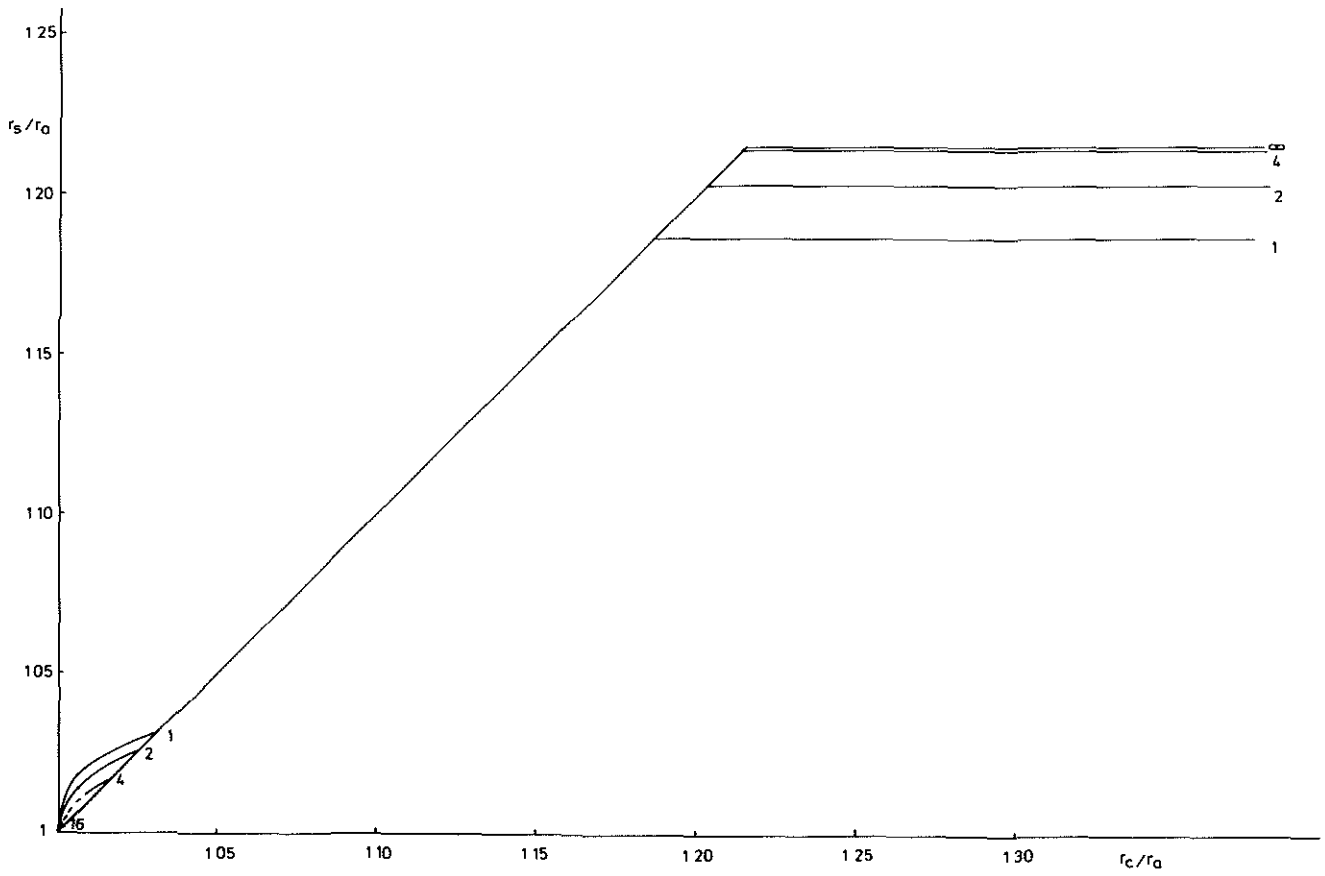

FIG. 8. Sonic radius versus critical radius, for $Z_i = 1, 2, 4, 16,$ and ∞.

TABLE I. Parameters β_l and η_c^* for several values of ion charge number

Z_i	β_l	η_c^*
1	1 46	1 80
2	3.85	1.85
4	6.54	1 95
16	9.68	2 0
∞	11.30	2.05

The flux-limit factor f has been discussed in detail in the literature; while theory suggests that $f \simeq 0.6$, some experiments and numerical simulations could only be explained for values of f sensibly smaller.[9]

Assume now Z_i to be large; Eq. (8) decouples from (6) and (7), and they simplify into

$$\frac{1}{2}\left(1-\frac{\theta_e}{u^2}\right)\frac{du^2}{d\eta}=\frac{2\theta_e}{\eta}-\frac{d\theta_e}{d\eta}, \tag{15}$$

$$\tfrac{5}{2}\theta_e+\tfrac{1}{2}u^2=-\bar{q}+\overline{W}H(\eta). \tag{16}$$

Here $\bar{q}$ may take either one of two forms:

$$\bar{q}_{cl}\equiv -\beta\eta^2\theta_e^{5/2}\frac{d\theta_e}{d\eta},$$

$$\bar{q}_s\equiv -\left(\frac{m_i}{Z_i m_e}\right)^{1/2} f\frac{\theta_e^{3/2}}{u}\,\mathrm{sign}\left(\frac{d\theta_e}{d\eta}\right).$$

The solution to Eqs. (15) and (16) should satisfy obvious conditions: defining the function $\sigma\equiv\bar{q}_{cl}/\bar{q}_s$, we should have $\sigma<1$ in the regions where the classical flux was used, and $\sigma>1$ where the flux was saturated. Because of the continuity of the heat flux (except at η_c), we also required that $\sigma=1$ on the classical side of any boundary between classical and saturated regions.

The problem to be solved is similar to those in the previous section and in Ref. 7: Choosing η_c freely in the range $(1,\infty)$, we must determine $u(\eta_c)$ and the eigenvalues β and $\overline{W}$; then Eqs. (9)–(11) [where now $Z_i(Z_i+1)^{-1}\simeq 1$] will yield $\mu(\eta_c)$, $P_a(\eta_c)$, and $W(\eta_c)$, from which $\mu(P_a)$ follows. It is worth stressing beforehand a few points proved in Ref. 4: (1) Both near $\eta=1$ and $\eta\to\infty$ heat conduction must be classical; (2) the Mach number $M=u/\theta_e^{1/2}$ at η_c^+ cannot be less than unity (and grows with η for $\eta>\eta_c$); and (3) if there is a saturated region within the interval $1<\eta<\eta_c$, Eq. (16) with $H=0$ and $\bar{q}=\bar{q}_s$ leads to $M=M_s$, where

$$M_s\left(1+\frac{M_s^2}{5}\right)=\frac{2}{5}\left(\frac{m_i}{m_e Z_i}\right)^{1/2} f. \tag{17}$$

The last two points show that if $M_s<1$, there must exist a discontinuous jump from subsonic to supersonic flow.

Here, we only analyze the range $M_s>1$. Notice that Z_i is some appropriate mean value of several ionization levels, which may be of order of 10 for typical ablators; we assumed $Z_i \gg 1$ (large ion mass number A_i) to simplify the analysis (the assumption $T_i=T_e$ of Ref. 4 leads to errors unless Z_i is large). For the ablative regime of interest, and A_i large, full ionization may not occur throughout the corona, the less so in the overdense, low-temperature, classical region at the boundary of which condition (17) is established: for $Z_i \simeq A_i/2$, $Z_i \simeq A_i/3$, and $Z_i \simeq A_i/4$, we get $f(M_s=1)\simeq 4.95\times10^{-2}$, 4.04×10^{-2}, and 3.50×10^{-2}, respectively. Thus, the restriction $M_s>1$ corresponds roughly to condition $f>0.04$, allowing for most of the range $0.03<f<0.6$, considered in experiments and simulations. Furthermore if $M_s<1$ the problem that ensues is undetermined; in Ref. 4 the jump was assumed isothermal and an *ad hoc* relation between densities, ahead and behind, was used. For $0.03<f<0.04$ ($M_s \lesssim 1$), that model does not appear better than just extrapolating results from the range $f>0.04$. On the other hand, if M_s is small (f well below 0.04) the jump is large, implying substantial transformation from thermal into (macroscopic) kinetic energy; there are some doubts about the validity of such a model.

As shown in Sec. II, in the absence of a flux limit both β and the solution $[u(\eta),\theta_e(\eta)]$ up to η_c, could be found, for any η_c without recourse to the interval $\eta_c<\eta<\infty$. For $Z_i>46$, two η_c intervals could be distinguished: As η_c went from 1 to $\eta_{sl}(\simeq 1.215$ for $Z_i\to\infty$, see Fig. 8), the solution $[u(\eta),\theta_e(\eta)]$ changed, and β went from zero to β_l ($\simeq 11.3$, for $Z_i\to\infty$), although $M(\eta_c)\equiv 1$. On the other hand, for $\eta_c>\eta_{sl}$ neither β ($=\beta_l$), nor the solution (given in Fig. 2 of Ref. 7 for $Z_i\to\infty$, and called here $[u_0(\eta),\theta_0(\eta)]$) depended on η_c; defining $M_0(\eta)=u_0/\theta_0^{1/2}$, we had then $M(\eta_c)=M_0(\eta_c)>1$.

Consider then any f such that $M_s>1$ and let $\eta(M_s)$ be the root of the equation $M_0(\eta)=M_s$. If $1<\eta_c<\eta(M_s)$, neither β nor the solution up to η_c, and in particular $u(\eta_c)$, are modified by the flux limit: for $1<\eta_c<\eta_{sl}$, use of (9) and (11) to eliminate η_c yields $\mu(P_a)$, while for $\eta_{sl}<\eta_c$, Eq. (9) alone yields $\mu(P_a)$ because $\beta=\beta_l$. If $\eta(M_s)<\eta_c$, the flux limit does not modify the solution up to $\eta(M_s)$, while $M=M_s$ and (17) hold for $\eta(M_s)<\eta<\eta_c$; $\beta=\beta_l$ and again (9) alone yields $\mu(P_a)$. Hence the relation $\mu(P_a)$ is independent of f and is that given in Ref. 7.

To find $\overline{W}$ we must consider the interval $\eta_c<\eta<\infty$. We find that there are three different cases.

(a) Classical flux throughout the interval; as in Sec. II, $\overline{W}$ is found by requiring that $\theta_e\to 0$ as $\eta\to\infty$.

(b) Saturated flux up to, say, η_{cl}, and classical for $\eta_{cl}<\eta<\infty$; $\overline{W}$ is obtained by evaluating (16) at η_c^+ [$H=1$, $\bar{q}=\bar{q}_s=(m_i/m_e Z_i)^{1/2} f\theta_e/M$] and then η_{cl} is found by requiring $\theta_e\to 0$ as $\eta\to\infty$ [remember that for any tentative value of η_{cl}, the slope $d\theta/d\eta$ at η_{cl}^+ follows from the requirement $\sigma(\eta_{cl}^+)=1$].

(c) Classical flux up to, say, η_f, saturated for $\eta_f<\eta<\eta_{cl}$, and classical again for $\eta_{cl}<\eta<\infty$. For $\overline{W}$ chosen within some range the solution, starting classical, saturates at a value $\eta_f(\overline{W})$ such that $\sigma=1$ at $\eta_f^-(\overline{W})$; $\overline{W}$ and η_f are determined from the condition $d\sigma/d\eta=0$ at $\eta_f^-(\overline{W})$, and then η_{cl} follows in the manner of (b). To justify the condition $d\sigma/d\eta=0$ at η_f^-, we evaluate the trivial equality

$$\bar{q}_s\frac{d\sigma}{d\ln\eta}=\frac{d\bar{q}_{cl}}{d\ln\eta}-\sigma\frac{d\bar{q}_s}{d\ln\eta}\quad\text{at}\quad\eta_f^-,$$

using $\bar{q}_{cl}=\overline{W}-\theta_e(5+M^2)/2$, $\bar{q}_s=(m_i/m_e Z_i)^{1/2} f\theta_e/M$, and Eq. (15) to obtain $d\bar{q}_{cl}/d\ln\eta$ and $d\bar{q}_s/d\ln\eta$ for $\eta<\eta_f$, and using (16) with $H=1$ and $\bar{q}=(m_i/Z_i m_e)^{1/2} f\theta_e/M$ and again (15), to obtain

$$\left.\frac{d\ln\theta_e}{d\ln\eta}\right|_+ = 4\,\frac{(m_i/m_eZ_i)^{1/2}f - M^3}{3M^3 - 5M + (3M^2-1)(m_i/Z_im_e)^{1/2}f}. \tag{18}$$

We finally arrive at

$$\bar{q}_s\left.\frac{d\sigma}{d\ln\eta}\right|_- = \frac{3M^3 - 5M + (m_i/Z_im_e)^{1/2}f(3M^2-1)}{2M(M^2-1)} \times \left.\frac{d\theta_e}{d\ln\eta}\right|_- (\sigma^+ - 1). \tag{19}$$

Since $d\ln\theta_e/d\ln\eta|_+$ should be negative, and $M \geqslant M_s > 1$, the denominator in (18) is non-negative; then the left- and right-hand sides of (19) must be non-negative and nonpositive, respectively. Hence $\sigma^+ = 1$, and $d\sigma/d\eta|_- = 0$.

Figure 9 shows the correspondence between f, W values and the different sequences of classical and saturated regions (for both $\eta < \eta_c$ and $\eta > \eta_c$). Figures 10 and 11 show P_a and r_c vs W for several values of f.

IV. DISCUSSION

A. Arbitrary ion charge number

If Z_i is not large the ion temperature is coupled to other fluid variables. Fluid profiles for $Z_i = 1$ are shown in Fig. 2. Complete results are given in Figs. 3–5 in dimensionless form. It is convenient to introduce the speed

$$V\left(r_a, n_c, \frac{m_i}{Z_i}, Z_i\right) \equiv \left(\frac{r_a n_c}{m_i/Z_i}\,\frac{k^{7/2}}{\bar{K}(Z_i)}\right)^{1/4}. \tag{20}$$

The horizontal axis of Fig. 3 is $W/r_a^2\rho_c V^3(Z_i = 1)$ and that of Figs. 4 and 5 is $P_a/\rho_c V^2(Z_i = 1)$; here $\rho_c \equiv n_c m_i/Z_i$. The vertical axis of Fig. 4 is $\dot{m}/4\pi r_a^2\rho_c V(Z_i = 1)$, $\dot{m}$ being the mass ablation rate $4\pi m_i\mu/Z_i$; the vertical axis of Fig. 3 is $[1.17\,P_a/\rho_c V^2(Z_i = 1)]/[W/4\pi r_a^2\rho_c V^3(Z_i = 1)]^{2/3}$.

Results for particular conditions are given in Figs. 6 and 7 in dimensional form. As Z_i goes from 1 to 16, $\dot{m}$ and P_a change at most by 25% and 30%, respectively; T_e and T_i at r_c change by about 60% and 600%, respectively. Figures 3–7 show that using Z_i independent of position is an approximation that should hardly affect the results except for $T_i(r_c)$, and to some extent for $T_e(r_c)$ and $P(r_c)$.

Figure 8 shows the sonic radius r_s versus the critical radius r_c. For Z_i below some value ($Z_i < 47$) the flow at r_c is subsonic if r_c/r_a is close to unity. For r_c/r_a such that $r_c > r_s$ (Fig. 8), Eq. (9) yields

$$\dot{m}/4\pi r_a^2\rho_c V = (P_a/\rho_c V^2)^{5/6}\,Z_i^{5/6}/(1+Z_i)^{5/6}\beta_i^{1/6}, \tag{21}$$

β_i given in Table I; $[Z_i^5/(Z_i+1)^5\beta_i]^{1/6}$ ranges from 0.527

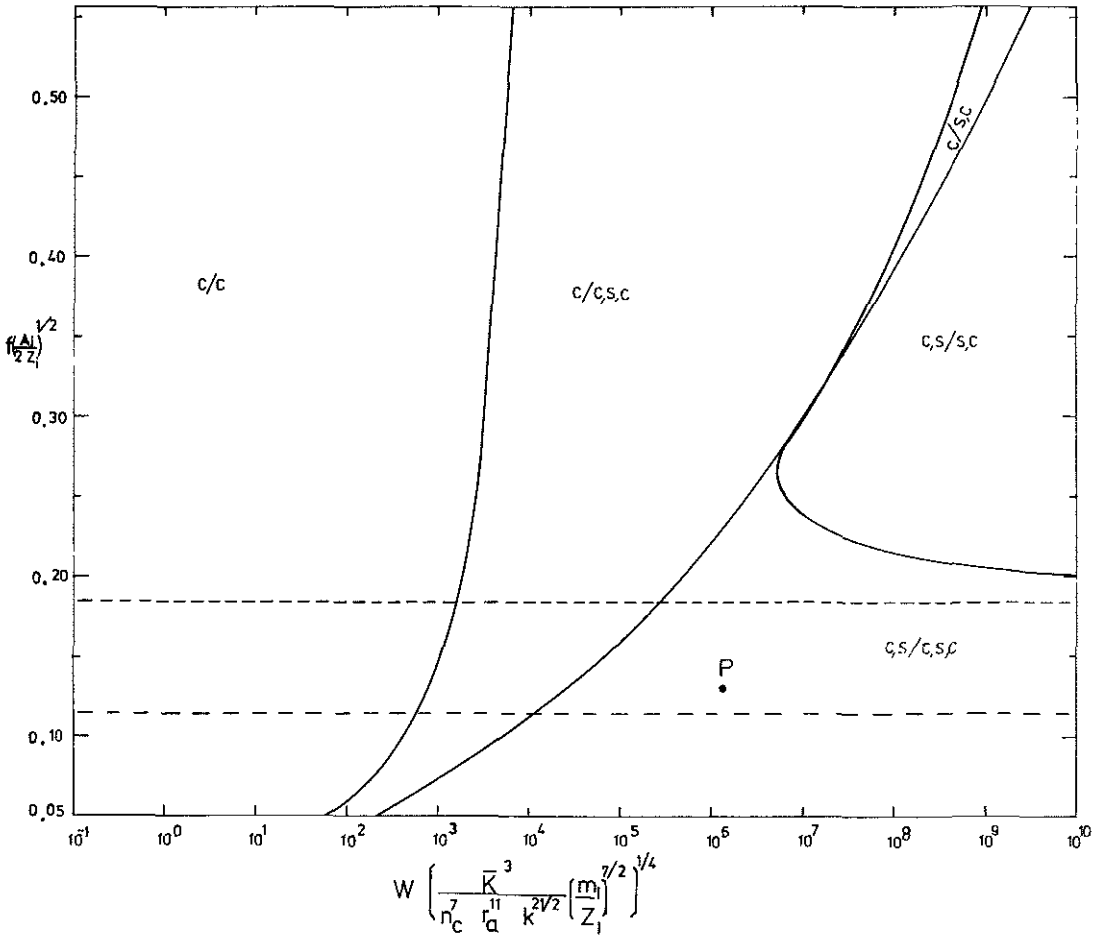

FIG. 9. Sequences of spatial regions with classical (c) and saturated (s) heat flux, in terms of flux limit f and laser power W; horizontal axis differs from that in Fig. 3 by the factor $[\bar{K}(Z_i)/\bar{K}(1)]^{3/4}$, $\bar{K}$ ≡Spitzer's heat-conductivity factor. For the conditions, for instance, of point P, the overdense flow presents two regions, classical next to r_a and saturated next to r_c; the underdense flow is classical next to r_c, and far enough from the pellet, and saturated inbetween. The solidus marks the critical radius r_c. – – – $M_s^2 = 5$, – · – $M_s^2 = 3$, in Eq. (17).

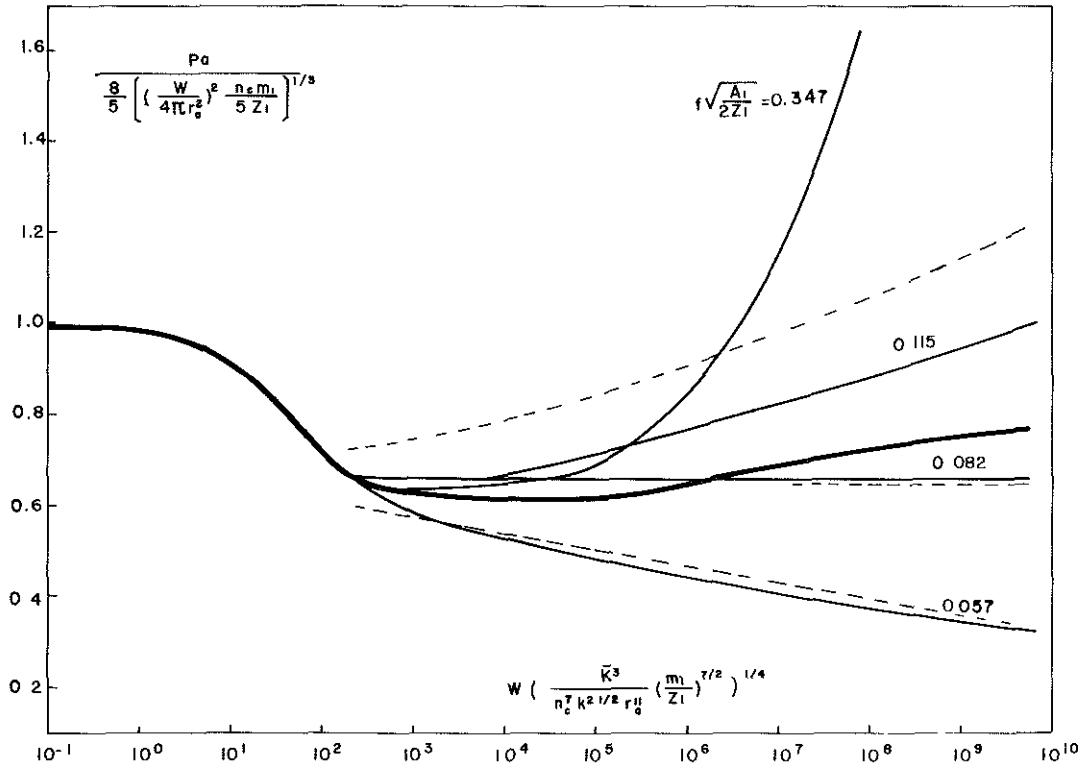

FIG. 10. P_a vs W for several values of f; results from Ref. 4 (– – –) and Ref. 7 (gross full line, no saturation considered) also shown. The vertical axis differs from that in Fig. 3 by factor $5^{4/3}/8 \times 1.17$; same horizontal axis as in Fig. 9.

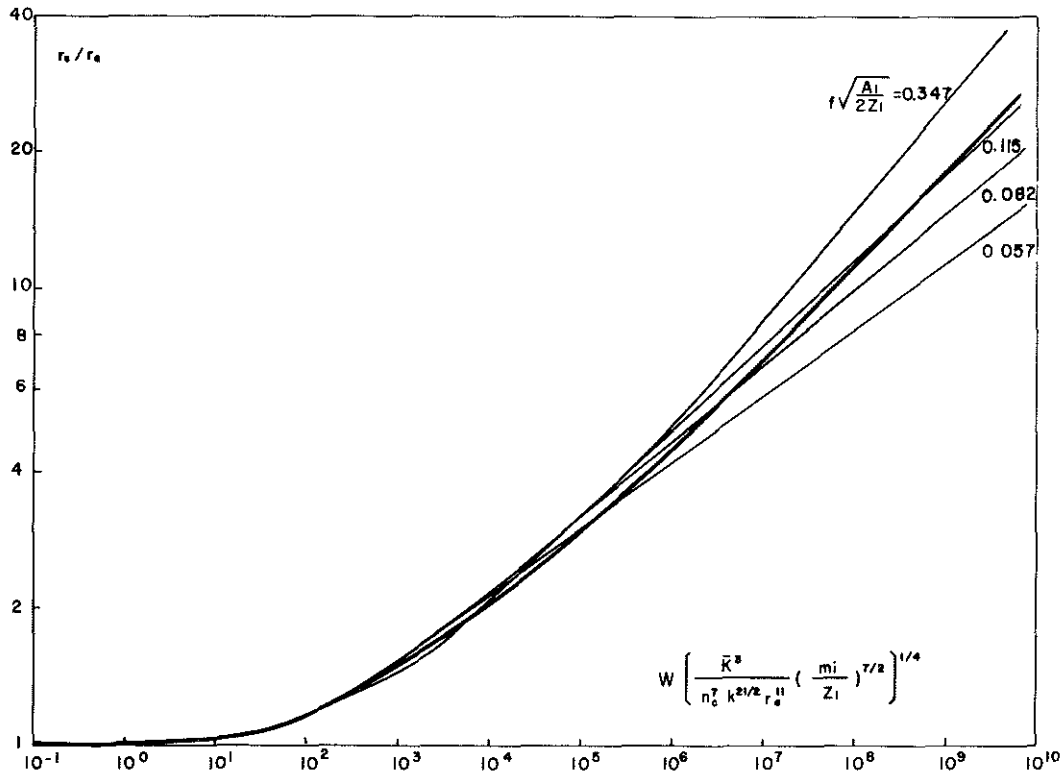

FIG. 11. Ratio r_c/r_a vs W for several values of f; results from Ref. 7 (gross full line) also shown. Same horizontal axis as in Fig. 9.

at $Z_i = 1$ to 0.668 at $Z_i = \infty$. For $r_c/r_a \to 1$ heat conduction is restricted to a thin deflagration layer. A rigorous analysis of such layers[10] (detailed in Ref. 7 for $Z_i \to \infty$) gives

$$\dot{m}/4\pi r_a^2 \rho_c V = (5n_d/8n_c)^{1/2}(P_a/\rho_c V^2)^{1/2},$$

$$P_a/\rho_c V^2 = (128n_d/125n_c)^{1/3}(W/4\pi r_a^2 \rho_c V^3)^{2/3},$$

where n_d is the density on the underdense side of the layer; $(125n_c/128n_d)^{1/3}$ ranges from 1.17 at $Z_i = 1$ to $5^{4/3}/8$ at $Z_i = \infty$ (Ref. 10).

Results in Ref. 2, which only apply for $r_c > r_s$, were given in terms of values of physical variables at r_s. To conveniently relate those results to ours we now give the relevant sonic values, from our analysis,

$$r_s/r_a = 1.215, \quad P_s/\rho_c V^2 = (\theta_s^{1/2} r_a^2/r_s^2) P_a/\rho_c V^2,$$

$$Z_i k T_{es}/m_i V^2 = \theta_s \beta_l^{1/3} (P_a/\rho_c V^2)^{1/3},$$

$$n_s = P_s/kT_{es},$$

$\beta_l \simeq 11.3$, $\theta_s \simeq 0.42$ (Fig. 2, Ref. 7); $P_a/\rho_c V^2$ can be obtained from Fig. 10 (gross full line). To write the preceding equations we assumed Z_i large, for which case the hypothesis $T_i = T_e$ of Ref. 2 is unimportant (except for the determination of T_i). The parameter "M" introduced in Ref. 2 should be set equal to 2/3.

B. Heat flux saturation

To analyze saturation we considered Z_i large. Figure 9 shows the sequence of spatial regions with classical and saturated flux, in terms of the dimensionless parameters of the problem, $f(A_i/2Z_i)^{1/2}$ and $W/r_a^2 \rho_c V^3$; Fig. 10 shows $P_a(f, W)$.

Equation (17) can be written as $2\phi = M_s(1 + M_s^2/5)$, $\phi \simeq 12.1 f(A_i/2Z_i)^{1/2}$, a quantity used in Ref. 4. It was assumed there that $M_s^2/5 \ll 1$, while we considered $M_s^2 > 1$; thus, the analyses are somehow complementary. Actually in Ref. 4, its analysis was assumed valid up to $\phi \simeq 1$ [$M_s^2 = 2$, $f(A_i/2Z_i)^{1/2} \simeq 0.082$]; our Fig. 10 confirms this. Agreement with simulations was found up to $\phi = 1.4$[4] [$M_s^2 = 3$, $f(A_i/2Z_i)^{1/2} \simeq 0.115$], where we find some disagreement (Fig. 10). Results from Ref. 4 should not be used above $M_s^2 = 3$, marked in Fig. 9. They should not be used either for W too low (r_c/r_a too close to unity): Fig. 9 shows that the sequence (*c, s/c, s, c*) (see caption to Fig. 9 for symbols explanation), considered in Ref. 4 for $M_s^2 < 5$, has a restricted range of validity. [For $M_s^2 > 5$, Ref. 4 discussed only the sequence (*c, s/s, c*).] To conclude we note that recent spherical experiments[11] suggest f values higher than those found in planar geometry.

The result for $P_a(W)$ obtained when saturation is not considered[7] ($f \to \infty$) is also drawn in Fig. 10 which shows that for a given power W saturation may decrease (low f) or increase (high f) the pressure P_a relative to the value attained when $f \to \infty$. The explanation of this result lies in a fact recalled in Sec. I: for $f \to \infty$ and r_c/r_a large most of the energy absorbed is lost by outward conduction.[7] Hence, for high f (weak flux inhibition) only this huge outward loss is inhibited, increasing P_a, while for f low enough the inward heat flux is strongly inhibited, reducing P_a. This leads to a second, seemingly paradoxical effect, seen in Fig. 10, too: In some cases a decrease in f, with W fixed, affects more strongly flux inhibition in the underdense flow, resulting in a higher P_a (or a lower W for given pressure).

Figure 10 shows that for some values of f,

$$P_a/[(W/r_a^2)^2 n_c m_i/Z_i]^{1/3} \simeq \text{const.} \tag{22}$$

This is not a trivial result, required by dimensional arguments; the left-hand side of (22) could have been any function of the abscissa,[12] or alternatively, of the ratio r_c/r_a [for instance, r_c could figure instead of r_a in (22)]. Nuckolls, in fact, suggested[6] $P_a[(W/r_a^2)^2 n_c m_i/Z_i]^{-1/3} \simeq (r_c/r_a)^{2/3}$, which would only be right for f high enough. In Ref. 4, emphasis was laid on low values of f, for which the left side of (22) decreases with growing W.

Figure 11 shows that r_c/r_a is weak function of the flux-limit factor. We also find that P_a/P_c and T_{ic}/T_{ec} decrease with f, and that the relation $\dot{m}(P_a)$ is not affected by saturation. We had found earlier [Eq. (21)] that for $r_c > r_s$, $\dot{m}(P_a)$ was independent of n_c and nearly so of Z_i: $\dot{m} \propto (A_i/Z_i)^{7/12} r_a^{11/6} P_a^{5/6}$. Since $r_a(t)$ will follow from $\dot{m}(r_a, P_a)$ and the pressure law $P_a(t)$, once this law is selected the ablation rate $\dot{m}(t)$ appears to be unaffected by conditions in the corona.

When the analysis of Ref. 4 is valid, the parameter $\hat{\sigma}$ introduced there is approximately $1.3 \times 10^{-4}\, \phi^{-7/3} (W/r_a^2 \rho_c V^3)^{4/3}$. Note that the ratio $W/r_a^2 \rho_c V^3$ (horizontal axis of Figs. 9–11) covers a very large range of values; for $1000 > r_a(\mu m) > 50$ (beginning and end of compression), $0.35 < \lambda(\mu m) < 10.6$ (third harmonic of Nd and CO_2), $Z_i = 10$, $A_i \simeq 2Z_i$, and a single power (10^{13} W) whose ratio ranges from 40 to 2.3×10^{10}. The influence of inverse bremsstrahlung for low values of $W/r_a^2 \rho_c V^3$, and hot electrons for high values is considered elsewhere.[13]

ACKNOWLEDGMENTS

This research is partly based on a doctoral thesis by J. Sanz, and was performed under the auspices of the Junta de Energía Nuclear of Spain.

[1] A. Caruso, Plasma Phys. **18**, 241 (1976).
[2] S. J. Gitomer, R. L. Morse, and B. S. Newberger, Phys. Fluids **20**, 234 (1977).
[3] Yu. V. Afanas'ev, E. G. Gamalii, O. N. Krokhin, and V. B. Rozanov, Zh. Eksp. Teor. Fiz. **71**, 594 (1976) [Sov. Phys. JETP **44**, 311 (1977)].
[4] C. E. Max, C. F. McKee, and W. C. Mead, Phys. Fluids **23**, 1620 (1980).
[5] L. L. Cowie and C. F. McKee, Astrophys. J. **211**, 135 (1977).
[6] J. H. Nuckolls, in *Laser Interaction and Related Plasma Phenomena*, edited by H. Schwarz and H. Hora (Plenum, New York, 1974), Vol. 3B, p. 399.
[7] J. Sanz, A. Liñán, M. Rodríguez, and J. R. Sanmartín, Phys. Fluids **24**, 2098 (1981).
[8] As in Ref. 7, we find that there is a value η_c^* such that, at large values of η, θ_e behaves as $\eta^{-4/3}$, $\eta^{-2/5}$, and $\eta^{-2/7}$ for η_c less than, equal to, and greater than η_c^*, respectively.
[9] W. Kruer, Comments Plasma Phys. **5**, 69 (1979).
[10] J. R. Sanmartín and A. Barrero, Phys. Fluids **21**, 1957 (1978).
[11] T. J. Goldsack, J. D. Kilkenny, B. J. MacGowan, P. F. Cunningham, C. L. S. Lewis, M. H. Key, and P. T. Rumsby, Phys. Fluids **25**, 1634 (1982).
[12] Actually dimensional arguments would introduce a second dimensionless parameter, $n_c r_a^3$, which, however, appears nowhere in the results.
[13] J. R. Sanmartín, R. Ramis, J. L. Montañés, and J. Sanz (to be published), J. A. Nicolas and J. R. Sanmartín (to be published).